Physica E 127 (2021) 114469

Contents lists available at ScienceDirect

Physica E: Low-dimensional Systems and Nanostructures

journal homepage: http://www.elsevier.com/locate/physe

Miniaturization design of all-optical encoder based on surface design and radiation source control

Debao Zhang [a], Guanjun You [a,b,*]

[a] Shanghai Key Lab of Modern Optical System, University of Shanghai for Science and Technology, Shanghai, 200093, China
[b] Terahertz Technology Innovation Research Institute, Terahertz Spectrum and Imaging Technology Cooperative Innovation Center, University of Shanghai for Science and Technology, Shanghai, 200093, China

ARTICLE INFO

Keywords:
All-optical encoder
Photonics crystal
Ring resonator
Photonic band gap

ABSTRACT

All-optical encoders with high response speed are required to achieve efficient information conversion in the field of ultra-fast information encoding, which can break the bottleneck of photoelectric conversion delay in traditional optical encoders and achieve a tunable bandwidth up to THz. The modifiable advantages of light path about all-optical encoder can widely satisfy the functional requirements of the modern high-precision device. This review introduces two principles of all-optical encoders, based on light propagation design and radiation source parameter design. We introduced the principle and miniaturization development of all-optical encoders based on the fabrication of two-dimensional (2D) photonic crystal defects to control optical path propagation, which can effectively use the photonic band gap effect to construct waveguide and the ring resonator to improve the coupling efficiency. In addition, we compared the previous method of the all-optical encoder with the design of radiation source parameters, and offer a practicable idea for the design of high-order encoder.

1. Introduction

Miniaturization is the promising direction of current smart device originating from the rapid development of integration technology [1,2,41]. Further reduction of the size will intensify the interaction between the electrons within the material after the integration level reaches the classical size limit of the material. The drastic movement of electrons causes a series of problems such as energy loss and device overheating, which influences the transmission rate of device information. This phenomenon has become a bottleneck in the miniaturization of traditional electronic devices [3]. The interaction between photons is weak compared with electrons, and the advantages of light in information transmission speed, bandwidth and capacity are obvious [4]. Therefore, light as the main carrier can greatly improve the information transmission speed and solve the problem of integration limit, and is widely used in the field of optical communication [5,6], such as frequency divider [7,8], encoder [9–11], filters [12–14], decoders [15,16], flip-flop [17], adder [18,19], comparator [20,21], etc. The encoder is a pivotal device in the information conversion process so that particularly important for its performance improvement.

Early optical encoders were mechanical, optical, and electrical displacement sensors [22–25], which had an inevitable delay during photoelectric conversion process. The speed of optical encoder has been close to the extreme after recent years of development, but it is hard to qualitative leap due to the existence of photoelectric conversion delay. All-optical encoder, a novel scheme only light as information carrier, has become the crucial device of the new generation of information encoding based on small size and low delay [26–30]. Photonic crystals (PhCs) consisted of different dielectric material is an artificial periodic structure, which has Bragg scattering phenomenon that modulates electromagnetic waves to cause periodic change of dielectric constant [31–36]. It allows electromagnetic waves in a specific frequency range to be reflected (impenetrable) in a specific direction of the PhCs, also known as photonic band gap (PBG). The PBG effect of PhCs is able to control the transmission of photons like electrons in semiconductor, and therefore become an important material for the manufacture of all-optical encoder [37–40].

All-optical encoder has two main encoding schemes from the perspective of control about the carrier of photons. One is to design material through dot or line defects to change the propagation path of light waves in the PhCs [41–50]. The characteristic of this coding method is the processing of the propagation path of the excitation beam. Its principle is to design the basic logic unit mainly by using the PBG and photon localization effect of the PhCs [51]. The main mode of beam

* Corresponding author. Shanghai Key Lab of Modern Optical System, University of Shanghai for Science and Technology, Shanghai, 200093, China.
E-mail address: gjyou@usst.edu.cn (G. You).

https://doi.org/10.1016/j.physe.2020.114469
Received 14 July 2020; Received in revised form 7 September 2020; Accepted 24 September 2020
Available online 30 September 2020

propagation in PhCs is the waveguide designed by line defects and the use of self-collimation effect, combined with the use of defect resonance cavity can effectively improve the coupling efficiency of the output and input ports. In addition, this all-optical encoder is divided into linear and nonlinear types based on the PhCs material characteristics and implementation methods [43]. However, this nonlinear process has narrow operating frequency range and requires a high-power energy , so nonlinear phenomena are more difficult to control than linear processes. Therefore, we will not elaborate on the nonlinear PhCs all-optical encoder in this article.

Another encoding scheme of the all-optical encoder mainly regulates the radiation core [52], which is characterized by the control of the radiation parameters rather than the need to design material. Thus, it can be more miniaturized than a defect-designed encoder. People can change the parameters (polarization, power, and wavelength) of the laser to interact with the material, and characterize the material's phenomena such as the luminous intensity or the parameter changes (polarization direction, waveform) for coding design [53,54]. This coding method can realize high order coding by adding extra excitation source as coding parameter. In addition, this speed of encoding is faster since there is no need to design the logic unit on the surface of the material, this encoder is faster. But the coding method is relatively complicated and few of study. We look forward to its brilliant performance in the field of ultra-fast information coding in the future [55,56].

The rest of the review is structured as follows. In section 2 we discussed the design principles of all-optical encoders with dot or line defects, introduced important design methods such as self-collimation effects, defect waveguides and ring resonator. Section 3 discusses the design principle of the radiation source control type all-optical encoder, and expands the high-order encoding method. Finally, in section 4, we draw a brief summary, discussing the evolution direction and application prospect of the miniaturization of the all-encoder.

2. Dot or line defect type of all-optical encoder based on 2D PhCs

Dot or line defects are artificially constructed on the surface of 2D PhCs, and PBG effect of PhCs is used to constrain the propagation path of specific wavelength beams, so as to achieve the principle of light regulation and design. We can use PhCs defects to fabricate a basic logic unit, and then combining specific encoding rules to design a high integrated, ultra-high speed all-optical encoder. In the design process, the ring resonator designed is used to improve the coupling efficiency and reduce the size by combining with the self-collimation effect. Finite difference time domain (FDTD) method can be used to solve the maxwell equation controlling this type of PhC [57–60], which can simulate the propagation and distribution of light wave in the PhCs in real time, and the transmittance spectrum can be obtained in a large range with Fast Fourier Transform (FFT) [61–63]. The method of Plane wave expansion (PWE) can be used to analyze the distribution of PBG diagram and equi-frequency contour (EFC) on the surface of the 2D crystal, and select the appropriate excitation source parameters. Next, the basic principle of 2D PhCs all-optical encoder is introduced [64–69].

2.1. Self-collimation effect

The self-collimation effect is a phenomenon that restricts the propagation of light waves in periodic structure, and realizes non-diffraction electromagnetic waves by utilizing the spatial dispersion characteristics of Bloch waves [47,70–73]. The effect does not need to construct a line-defect waveguide on the surface of the crystal, so that the light distribution of a specific wavelength can be in a state of collimation propagation. The designed encoder has a faster propagation speed because the self-collimation mode is located in the conduction band [74,75]. Due to the structure of the PhCs has periodic translational symmetry, we can use the PWE method to obtain the band structure diagram and EFC diagram, as shown in Fig. 1. (The radius and dielectric constant of the host Si rods are r = 0.35a ("a" is the lattice constant) and $\varepsilon = 12$ respectively).

The direction of energy flow determines the direction of beam propagation, while the direction of group velocity V_g represents the direction of energy flow. We can easily see from Fig. 1 that the V_g of each wave vector K is perpendicular to the equi-frequency plane at the frequency $f = 0.1942(a/\lambda)$ around [75]. Therefore, a beam satisfying specific frequency can be propagated in the direction of almost no diffraction, as shown in Fig. 2.

The self-collimation effect [76–82] can reduce the size of the all-optical encoder but the propagation direction is limited relative to the line defect waveguide. We can use the self-collimation effect of the PhCs to control the beam collimation propagation, and construct the reflector and beamsplitter with line defects to design a complete all-optical encoder [83,84].

2.2. Reflector and beamsplliter based on line defect

Making a suitable line defect radius design on 2D PhCs can realize the function of reflector and beamsplitter [75]. Change the size of the line defect rod on the propagation path of self-collimation beams and observe the changes in transmitted power and reflected power, as shown in Fig. 3. (The structure of 2D PhC is a square lattice array of silicon rods in air background. The dielectric constant and the refractive index of the dielectric rods are 11.97 and 3.46 respectively. The radius of the host rod is 0.35*a where "a" is the lattice constant).

We can see that when the defect radius is close to the host rod radius (no line defect), the transmitted power is close to the unit value. The

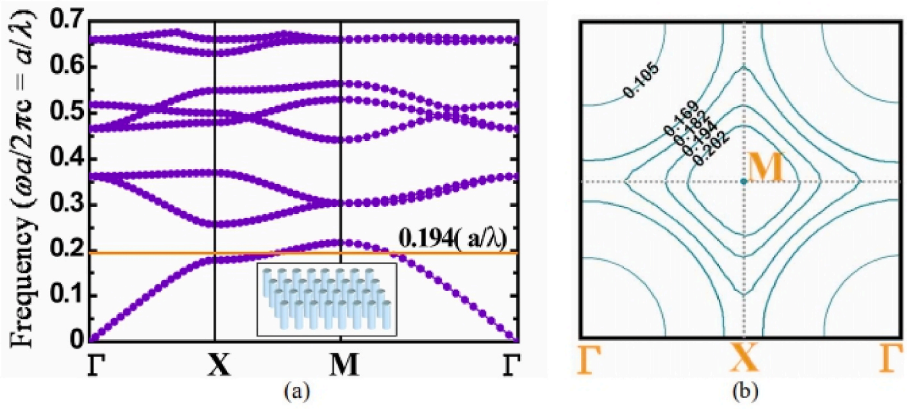

Fig. 1. The structure of 2D square lattice PhC is composed of Si rods in air background. (a) Band diagram of the PC structure for E-polarized mode (b) Equi-frequency contours of the first band. This picture is reproduced from Ref. [74].

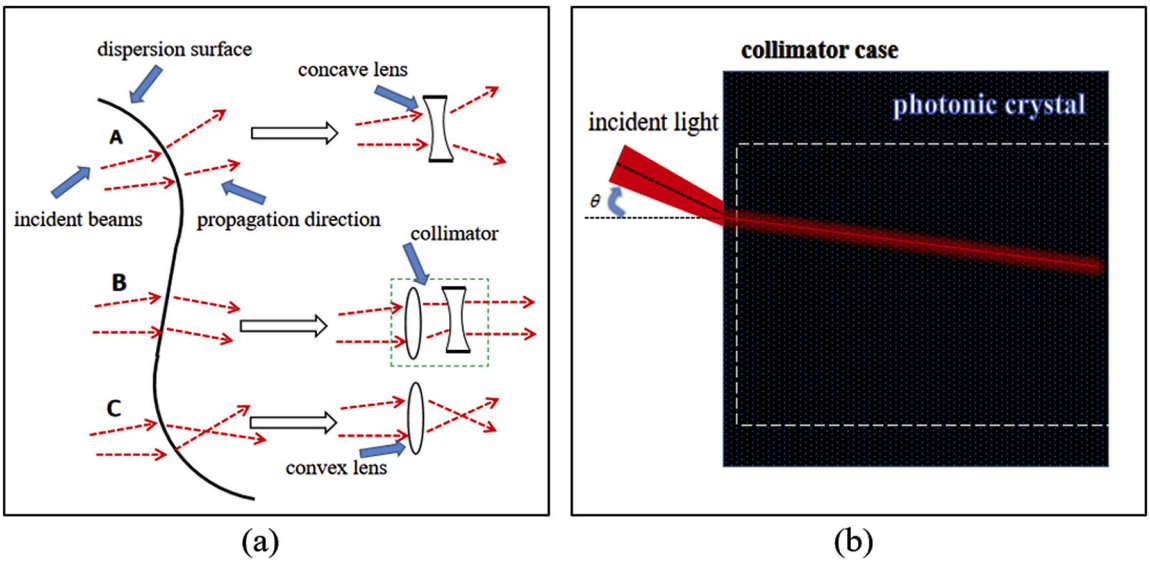

Fig. 2. (a) Three light propagation phenomena at dispersion surface. "**B**" is self-collimation phenomenon. (b)Self-collimation phenomenon occurred in PhC at a specific angle "θ".

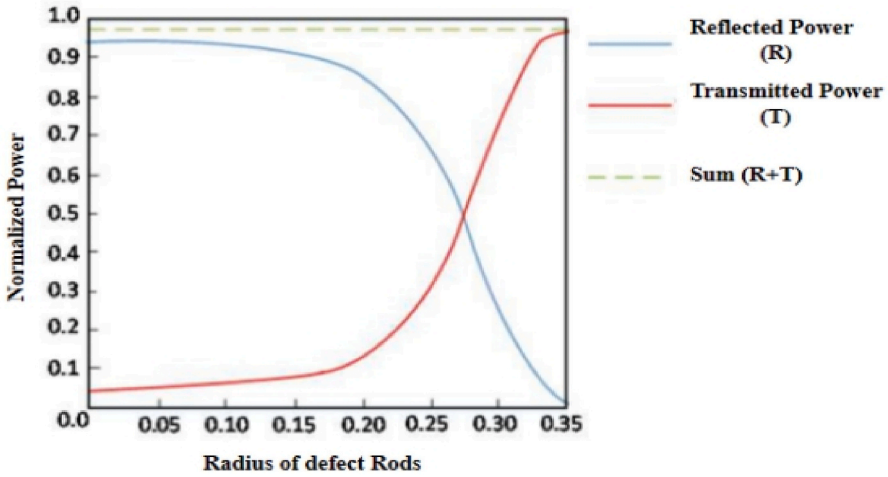

Fig. 3. The diagram of normalized power changes with the radius defect rod. This picture is reproduced from Ref. [75].

transmitted power decreases and the reflected power ratio increases as the defect radius decreases. When the defect radius is close to 0 (the rod is completely removed), the reflected power ratio is close to the unit value, which can be regarded as a reflector. We note in Fig. 3 that when the line defect radius is equal to 0.274R, the transmitted power ratio is equivalent to the reflected power, which can be regarded as a beamsplitter.

Fig. 4 is a case of a binary all-optical encoder designed using the self-collimation effect combined with a line defect reflector and a beamsplitter:

It is worth noting that there is a phase difference $\pi/2$ between the transmitted and reflected beams after the beam passes the beamsplitter designed by the line defect. For the defect radius larger than the host rod, the $-\pi/2$ difference between transmission and reflection, otherwise $\pi/2$. Therefore, the design of the encoder is the phase superposition or counteract of the two beams, which should be taken into account, as shown in Fig. 5.

2.3. Line defect waveguide and dot defect

Line defect waveguide is another constrained beam propagation effect in PhCs, which uses line defects to construct waveguide on the surface of PhCs [85–89]. The PhC waveguides use the principle of resonance matching in different directions, so as long as the defect mode matching is satisfied, it not only has high propagation efficiency for line waveguide but bend waveguide and branch waveguide. The photon is affected by the photon localization of the PhC, and it is bound in the waveguide with almost no energy loss during the propagation process. Three basic waveguide structures, as shown in the Fig. 6:

It has been proved that the three waveguides have higher propagation efficiency and no obvious energy loss under specific design matching [87,90–93].

The all-optical encoder whose optical propagation path is regulated only by the optical waveguide is shown in the Fig. 7:

This all-optical encoder has a delay time of 200 fs and an ultra-fast switching speed of 5 THz. The size is 880 μm^2including the supplemental input port I_0. The structure is simple and no ring resonator [94]. From Fig. 7 we can see that on the cross section where these waveguides are interconnected, a defect rod is placed at the end of each L-shaped waveguide to increase the number of light waves moving toward the output. In addition, reposition the dielectric rod to reduce retroreflection at the waveguide bend.

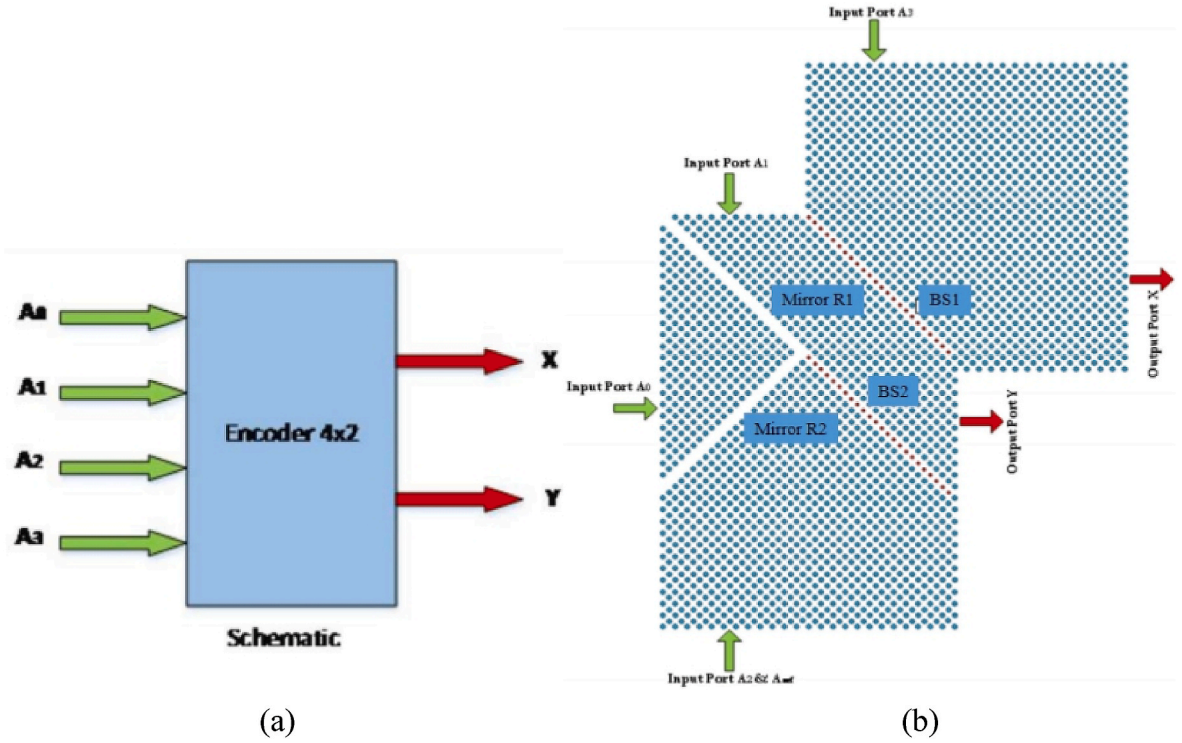

Fig. 4. Schematic diagrams (a) Simplified diagram of encoder pins (b) all-optical encoder manufactured by self-collimation effect and line defect reflector and beamsplitter. This picture is reproduced from reference [75].

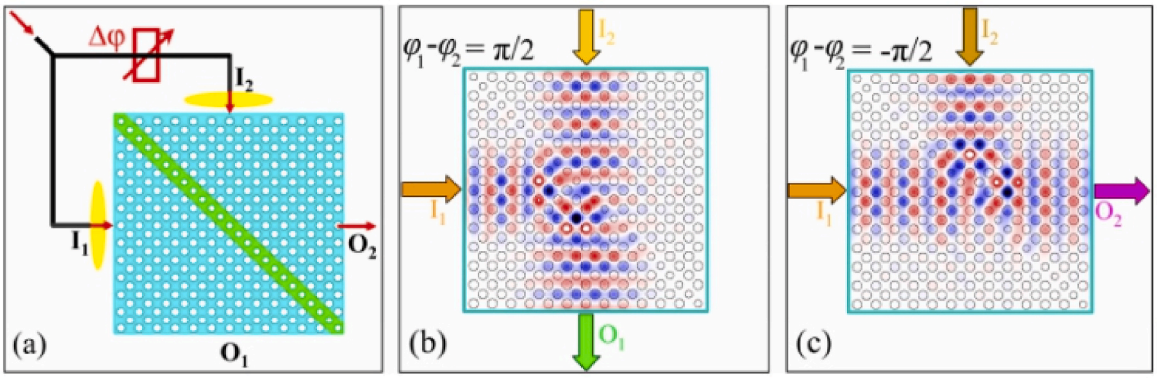

Fig. 5. (a) The phase of two laser beams (I_1 and I_2) of the same light source is adjustable, and the split beams with equal energy enter the PhC from perpendicular directions. (b) The phase difference is $\phi_1 - \phi_2 = \pi/2$ between I_1 and I_2, only O_1 output port has energy output. (c)The phase difference is $\phi_1 - \phi_2 = -\pi/2$ between I_1 and I_2, only O_2 output port has energy output. This picture is reproduced from reference [74].

The size and position of the defect rod determine the function of the dot defect. We introduce the functions of a-e in Fig. 8 respectively. The "a" and "b" have a symmetrical position structure, the radius is $r_a = r_b = 0.5r$ (r is the host rod radius), and its function is to prevent light from entering the input port end and reduce the return loss when the corresponding input port is closed. The "c" rod with a radius of $0.5r$ is shifted to the right by 0.5a ("a" is the lattice constant) to reduce energy loss. The "d" and "e" rods are offset by 0.1 μm in the horizontal and vertical directions, which is used to increase the output efficiency [96].

2.4. Ring resonators of PhCs

A ring resonator can be built in the PhC in order to improve the coupling efficiency between the input and output waveguides and decrease the cross reflection between the input ports. The ring resonator is formed by constructing ring line defects on the surface of the 2D crystal. It can be bound by the PBG effect of the PhC and combined with the design principle of the reflector in section 2.2 to form a wrapped reflector cavity with a high degree of coupling and a high Q factor [75, 97].

The common crystal microcavity is composed of dot defects, its resonance mode is single, and adjustment range is limited. When the microcavity is used for multiple wavelengths, the number of microcavities must be increased, which will greatly increase the energy loss. The ring resonator has multiple modes and can obtain multiple narrowband signals, which can make up for the disadvantages of ordinary microcavities. In the actual design process, we need to use ring resonators in combination with microcavities according to our own needs, because the size of the microcavity can be made very small. Using the electromagnetic calculation method of the FDTD, the propagation and distribution of beams in the ring cavity are simulated, and the optimization is carried out. According to the dielectric constant of the material

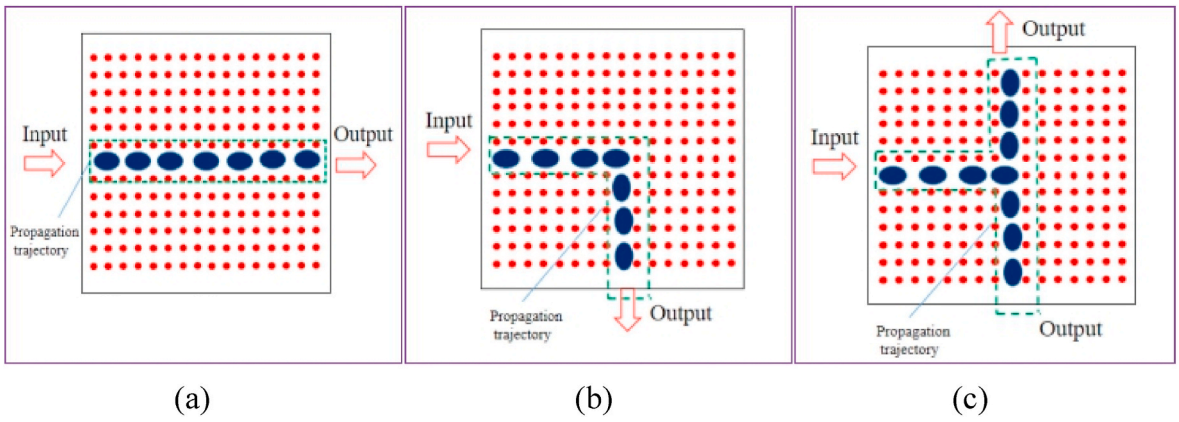

Fig. 6. The waveguide is constructed by line defects on the surface of the 2D PhC. (a) line waveguide (b) bend waveguide (c) branch waveguide.

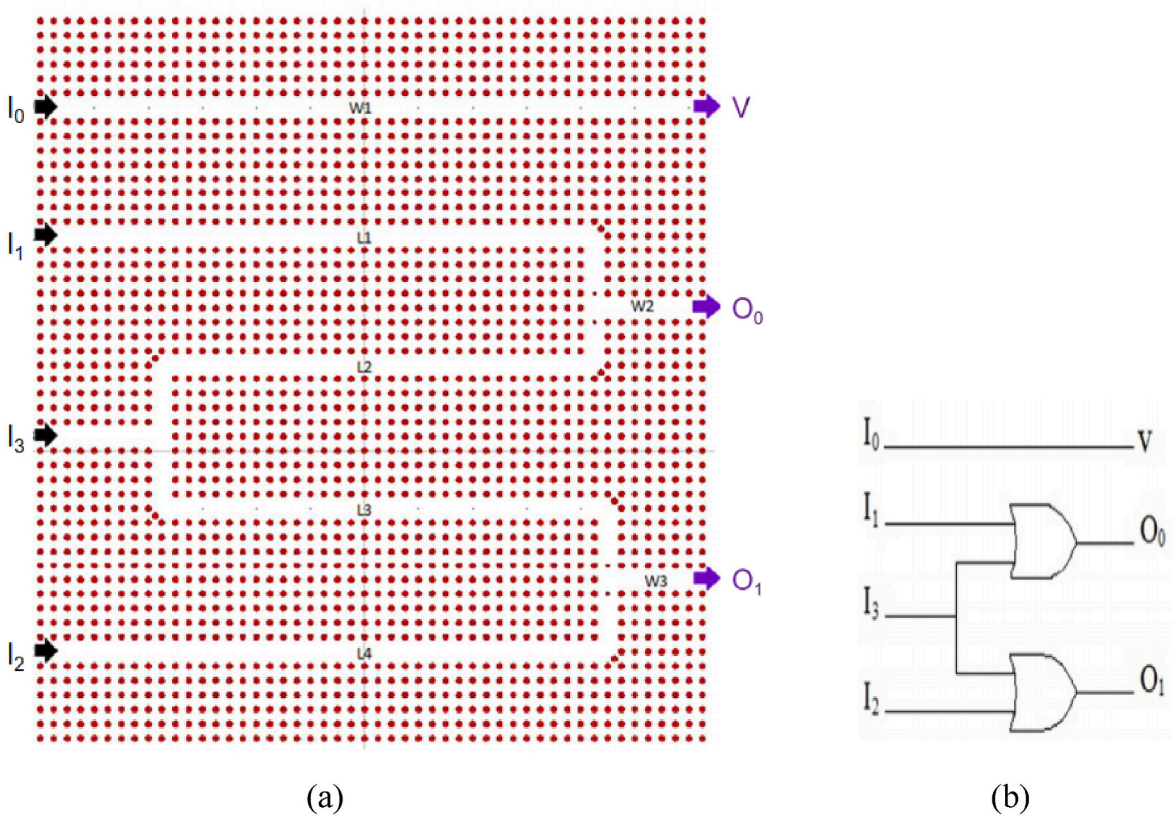

Fig. 7. (a) Structure diagram of all-optical encoder using only line defect waveguide (b) Functional logic diagram, this picture is reproduced from Ref. [94].

and the radius of the host rod, select the appropriate wavelength of the light beam, which is within the PBG. The appropriate ring resonator parameters are designed by changing the number of sides, the radius of the cavity and the width of the ring resonator. We repositioned the dielectric rod in order to eliminate the retroreflection of the curved part and improve the light guiding performance of the cavity at the bend of the ring resonator [98,99]. This method is similar to the bending of waveguides of section 2.3, as shown in Fig. 9.

The use of ring resonator is usually combined with waveguide propagation. Therefore, the interaction between ring resonator and waveguide needs to be considered within the design range. The coupling between the waveguide and the ring resonator needs to satisfy the common defect mode, so the ring resonator has the function of frequency selection [100]. Fig. 10 shows that changing the radius of the coupling rods can obtain different transmission effects.

The different propagation modes of light beams with different wavelengths in this design are shown in the Fig. 11:

We can clearly see that the 1550 nm light beam enters the ring resonator during the propagation of the linear waveguide. In addition, the ring resonator can be used to prevent the propagation of light waves in the linear waveguide, which we call the blocking effect [101] of the ring resonator, as shown in Fig. 12.

Obviously, the ring resonator of Input "A" prevents the beam of Input "B" from reaching the output "O" port. A reasonable use of ring resonator can greatly improve the performance of the all-optical encoder, but there are several aspects need to be noted. First of all, the volume of the ring resonator is much larger than that of the dot defect microcavity. Therefore, the use of ring resonators and the size design of single ring

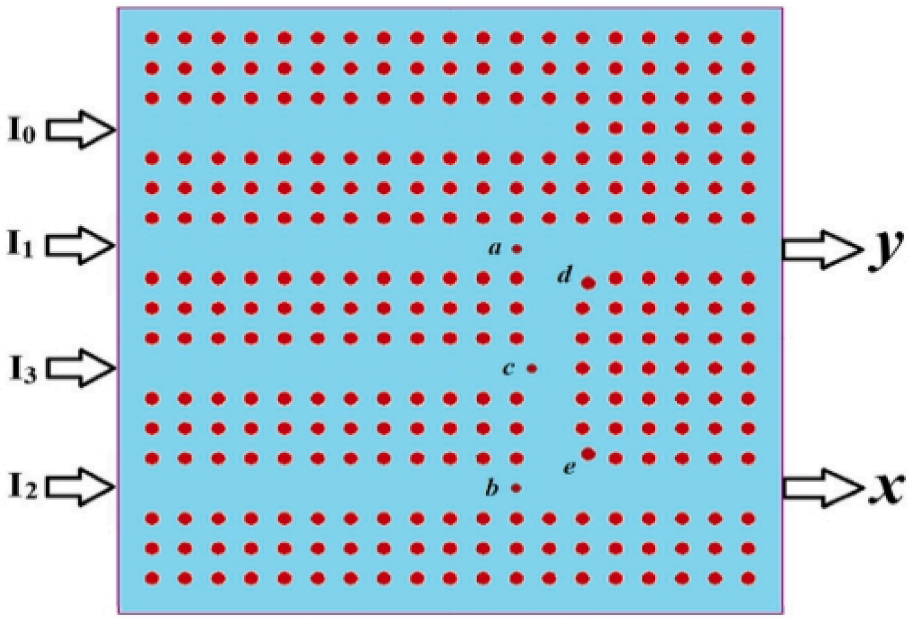

Fig. 8. The location map of different type dot defects in a complete 4 × 2 all-optical encoder. This picture is reproduced from reference [96].

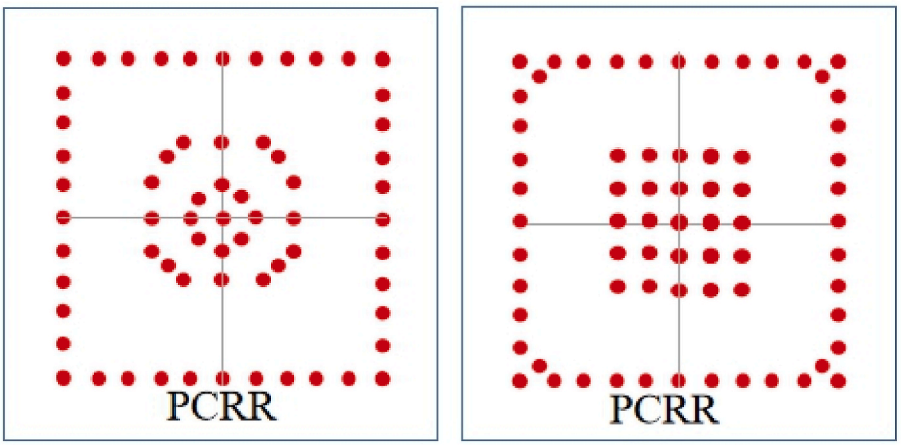

Fig. 9. Two basic bending ways of ring resonator, "PCRR" is PhC ring resonator. (a)Inner ring bending (b) Outer ring bending.

resonator should be reduced as much as possible in encoder design. Secondly, the ring resonator is composed of a ring line defect waveguide. Therefore, the PBG effect exists in the ring resonator, which limits the threshold of input power. Too high input power will lead to the ring resonator is difficult to bind, resulting in the destruction of coding performance. The input power range it can support is mainly related to the shape, size and material of the ring resonator. In all-optical encoders, ring resonators are usually used with line defect waveguides, so the threshold of input power should be considered as the whole encoder structure. A conventional method for selecting a reasonable encoder input power is discussed in the next section.

2.5. Miniaturized design discussion

The fundamental PhC structure used here to design the proposed logic gate and final all-optical encoder is a square lattice of dielectric rods in air background. The basic methods of crystal defect design are: remove, change the size, and move the host rod. A complete all-optical encoder, the main components include logic gates, combination rules and sequence circuits Thus, we can list truth tables or logical expressions according to our goal. The combination rules consist of basic logic gate units [29,42,44,95], and we can design basic logic units through defects design, as shown in Fig. 13:

It is relatively easy to simply implement the encoding function, but the difficulty is to design a low delay, ultracompact all-optical encoder. So, we optimize from several different aspects. The first step for all-optical encoders to regulate light beam is propagation. We can use the self-collimation effect or introduce line defect waveguides in the PhC. By designing T-shaped, Y-shaped or other shape waveguide structures to introduce the beam. We will reasonably use the ring line resonator to improve the coupling efficiency of the input and output and reduce the cross reflection between the input ports. In addition, in order to further improve the transmission efficiency, we have to eliminate the corner backward reflection in the design of the defect; We need to add additional corner dielectric rods at the corner. We can place a defect rod at the end of each L-shaped waveguide to increase the number of light

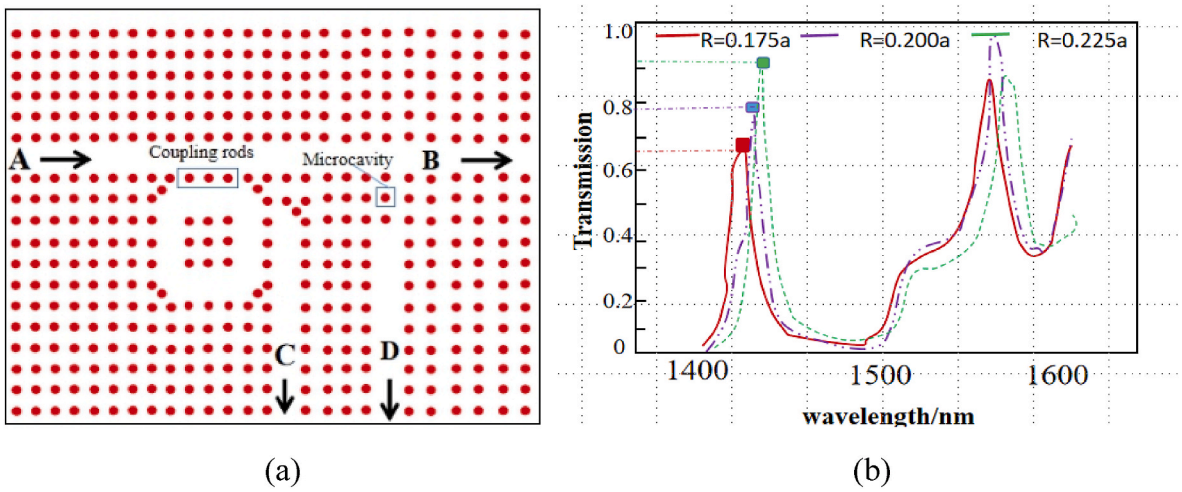

Fig. 10. (a) Three-wavelength PhC frequency selector (b) The transmission of PCRR characteristic diagram with different coupling rod radii R. Reproduced from reference [100].

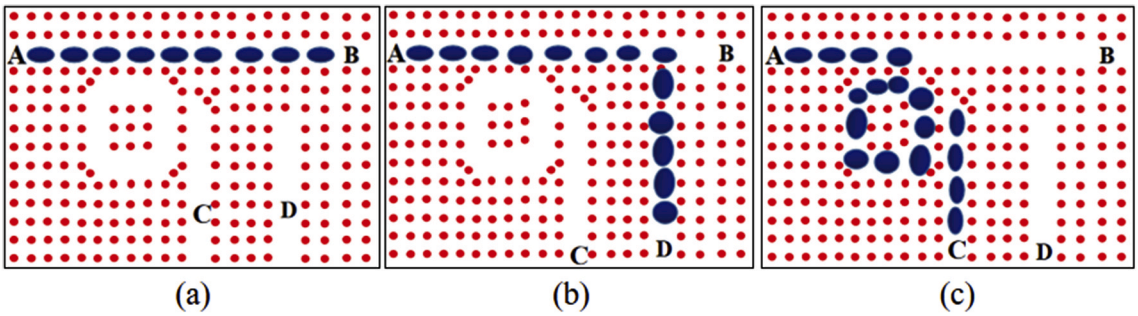

Fig. 11. (a) 1500 nm light field distribution diagram (b) 1550 nm light field distribution diagram (c) 1610 nm light field distribution diagram.

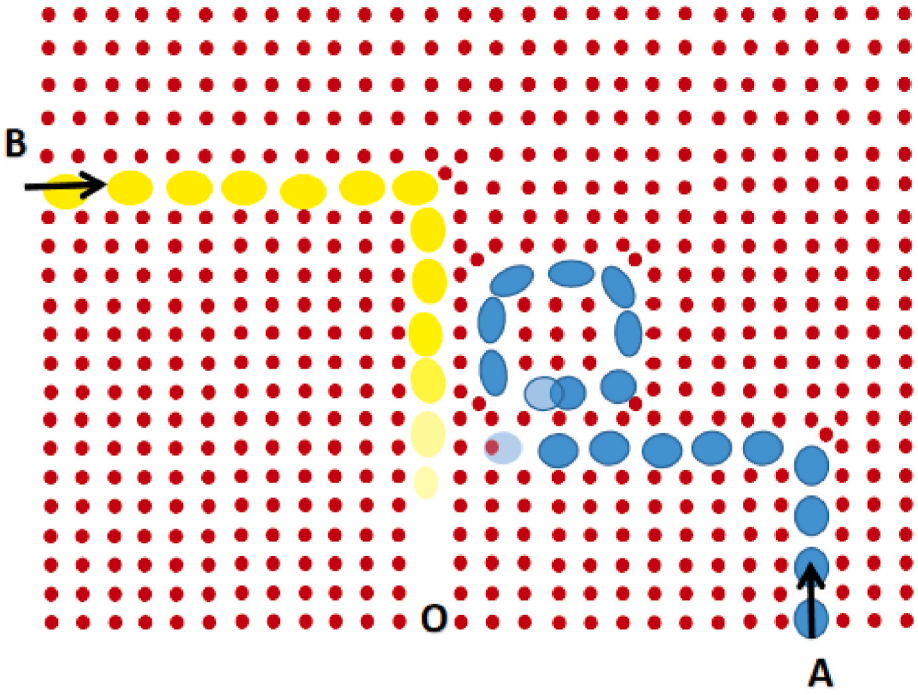

Fig. 12. The blocking effect of a ring resonator in 2D PhC.

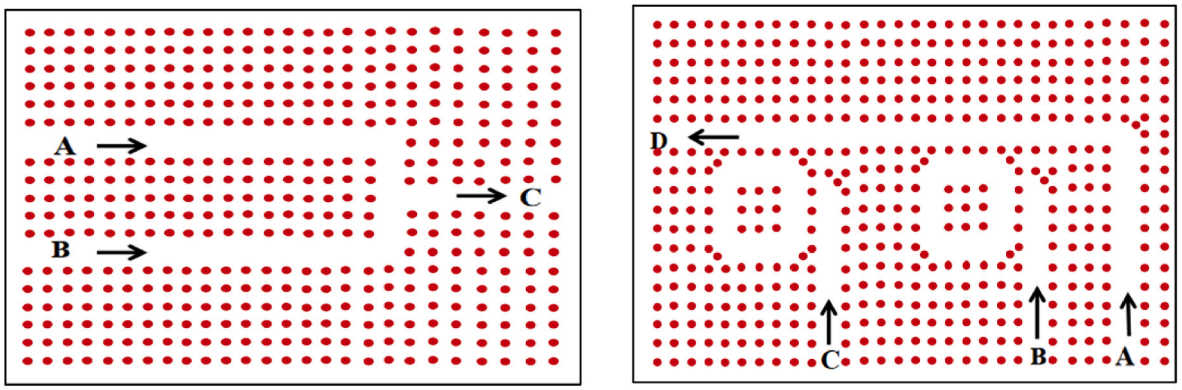

Fig. 13. Basic Logic unit (a) "OR" logic gate. (b) "NOR" logic gate.

waves moving toward the output waveguide on the cross-section of these waveguides connected to each other.

In the second step, we have to consider the material matching of light beams and PhCs. The first thing to consider is the bandgap structure of the material, which determines the selection effectiveness of the input light beam. The important factors of the band gap structure are the lattice constant, the size of the dielectric rod, the refractive index, etc. We use the FDTD method to solve the Maxwell's equations that control this PhC to simulate the propagation and distribution of light beams in real time, and we can obtain a large range of transmittance spectra at once with the help of FFT. Then the PWE method is used to solve the PBG distribution of the PhC [94]. Just use RSoft software to solve the equation (1):

$$-\sum_{G'} k(G-G')(k+G') \times \{(k+G') \times H_{kn}(G')\} = \frac{\omega_{kn}^2}{c^2} E_{kn}(G) \tag{1}$$

$$-\sum_{G'} k(G-G')(k+G') \times \{(k+G') \times E_{kn}(G')\} = \frac{\omega_{kn}^2}{c^2} H_{kn}(G)$$

where ω_{kn} is the angular Eigen frequency for E and H fields, G and G' are the reciprocal lattice vectors and k is the refractive index distribution function. In order to obtain faster switching speed and low delay time, we also need to select the radius matching of the rod of the ring resonator. Here is a rough method, according to the PBG to select the appropriate wavelength continuous wave (CW), as the input signal of a port. Then gradually change the inner radius of the dielectric rods of the ring resonator and measure their normalized power $P_n = P_o / P_i$ (the input power P_i and the output power P_o) respectively [102].

The more important step is to consider the actual application matching problem. The overall size of the all-optical encoder needs to be taken into account to achieve the integrated design of high-precision device. Using a simple method to multiplex the basic logic unit of the optical encoder. For example, the volume of ring resonators is relatively large in optical encoders, and the development direction is also to reduce the number of ring resonators into common resonators, as shown in the Fig. 14.

The upper picture is a good example of ring resonator multiplex in current [102]. The path used for waveguide propagation is also developing towards short distances, but it is worth noting that we cannot reduce the size so that the PBG of the material is difficult to restrain the propagation of photons. The energy loss of the propagation path also requires considering the width and length of the waveguide channel, as well as the interaction between the material and the light beam. Unfortunately, the output power of the encoder is very different, so it is not suitable to be used with multiple encoders in optical integrated system.

Generally, the uniform output power is also a noticeable parameter in order to improve the applicability of encoder in optical integrated circuit. When the output power difference of a single encoder is too large, it is difficult to combine with the input of the next encoder. Therefore, we introduce an effective output power selection method [106], which is based on the parameters of the material itself, the composition of the encoder, and more importantly, the effective selection of the input power. When the input power does not damage the encoder structure, change the different input power, as shown in Fig. 15. For case 2 and 3, it has symmetrical coding structure, so it has the same output effect. When the input power is equal to 1 mW/μm^2, the output power is similar, and there is a large contrast ratio at the same time. In this way, the output power of the encoder (in the mode of equivalent to the logical level one) can be used as the input signal of the next stage encoder in the integrated optical system.

Finally, an important evaluation criterion in all optical encoder is the maximum response time, which represents the time delay between the encoder input and the set logic "1" output power. In practical integrated optical system, the response time of each all-optical encoder or optical device affects the response time of the whole system. Therefore, we need to reduce the maximum response time of the encoder as much as possible in the design of all optical encoder. We conclude the encoder performance comparison of some references, such as Table 1.

In practical 2D all-optical encoder, especially the PhCs used for near-infrared communication, usually etch holes or rods in a heterostructure slab to ensure the light confinement in the vertical structure direction. At this time, in order to reduce the computational complexity of 3D FDTD, the effective index method (EIM) and 2D FDTD method can be combined to simulate the propagation of light beam in the encoder. The refractive index of dielectric materials is replaced by the EIM of guided mode in the 3D heterostructures without perturbation. It has been proved that the effective index method is applicable in a wide frequency range for photonic crystals with low refractive contrast [107,108].

The all-optical encoders based on 2D PhC designs are mainly binary 4 × 2 [96,98,102,103] or 8 × 3 [99,104] encoders, with 2^N input port and N output ports. The all-optical encoder is divided into linear [105, 106] and nonlinear [109]. The use of nonlinear Kerr effect to realize PhCs-based optical logic devices is an early common solution, relying on nonlinear materials, but requires high input power, narrow operating frequency range and difficult to integrate with silicon-based optical devices [110–116]. Therefore, all-optical encoders have mainly developed toward linear realization schemes in current. Under the premise of satisfying the actual function, our optical encoder design mainly considers aspects such as size, encoding speed, propagation efficiency, operable wavelength [45], and high-order encoding.

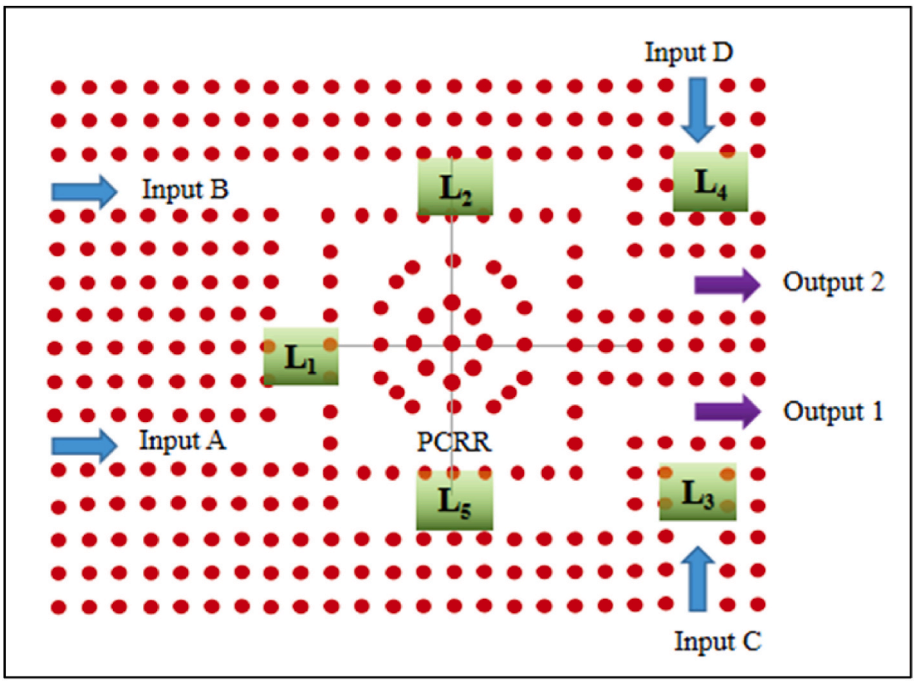

Fig. 14. An ultracompact all-optical encoder to multiplex the ring resonator.

3. Radiation source type of all-optical encoder based on perovskite microspheres

The encoder of the radiation source type is mainly based on the adjustment of the excitation parameters of the source to achieve the purpose of optical encoding [52,53]. Unlike the optical encoder described in the previous section, it does not require manipulation of the light propagation path on the surface of the PhC, so there is no need to design complex defect structures. This is a relatively novel design method of all-optical encoders. There are few relevant introductions at present, but it can be in obvious contrast with 2D PhC encoders. The all-optical encoder introduced next is based on perovskite microsphere (MS) materials, but is not limited to such materials. Only the radiation source parameters are adjusted, and the material structure is not required to be designed. Therefore, the size of this encoder can reach the sub-micron level, which solves the problem of the size limit of the 2D PhC encoder based on defects. We take a typical article as an example to expand the details [52].

Table 1
Response time comparison of PhCs all-optical encoders in some references.

Reference	Response time (ps)	Area (μm^2)
[75]	1.4	3795
[94]	0.2	880
[96]	~0.1	132.7
[101]	2000	1225
[102]	0.1	128.52
[106]	0.24	148

3.1. Degree of linear polarization switch

Changing the intensity of the excitation beam interacts with the material, and the different states (intensity, polarization, pulse shape, wavelength) that appear as coding parameters. All-inorganic halide lead cesium perovskite MS material, prepared by chemical vapor deposition at high temperature [117,118], which typical image of SEM dispersed

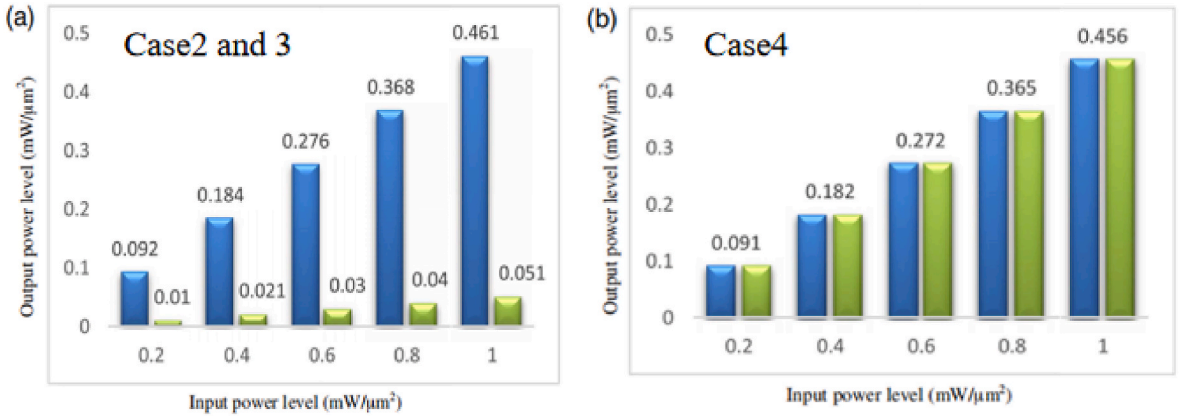

Fig. 15. Schematic diagram of output power of different cases under different input power (a) case 2 and 3 (b)case 4. Reproduced from Refs. [106].

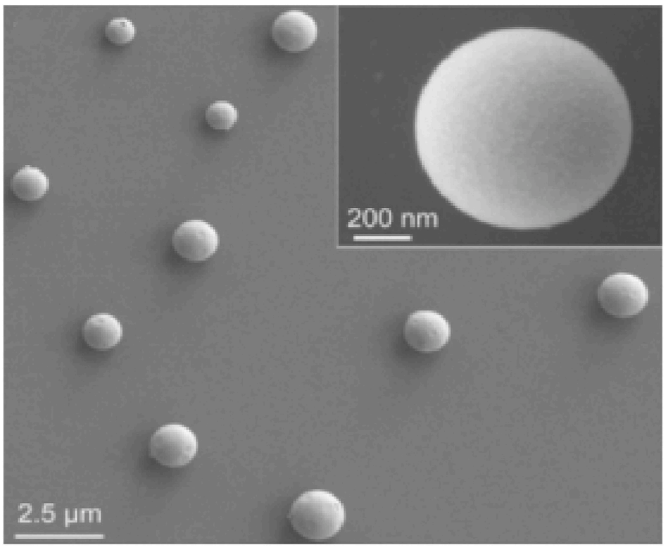

Fig. 16. The SEM image of all-inorganic halide lead cesium perovskite MS material. This picture is adapted from reference [52].

on a silicon substrate is shown in the Fig. 16.

The perovskite structure of this MS has been proven to have good crystallinity and lower defects, and the crystal structure is orthorhombic. The material itself can be regarded as a high-quality whispering gallery (WG) microcavity [119,120]. The influence of parallel and vertical beams with polarization directions on the Photoluminescence (PL) Spectroscopy of the material under the different power states are studied, as shown in the Fig. 17.

Obviously, there is a very sharp peak at the wavelength of 534.5 nm and an obvious threshold at the cavity resonance λ_c, which intuitively shows the high degree of linear polarization (DLP) of the stimulated radiation field.

The relationship between DLP and Pumping density at the threshold wavelength is shown in the Fig. 18:

The change in pumping intensity causes an abrupt jump in DLP, which is equivalent to two states of "On" and "Off" ("1" and "0").

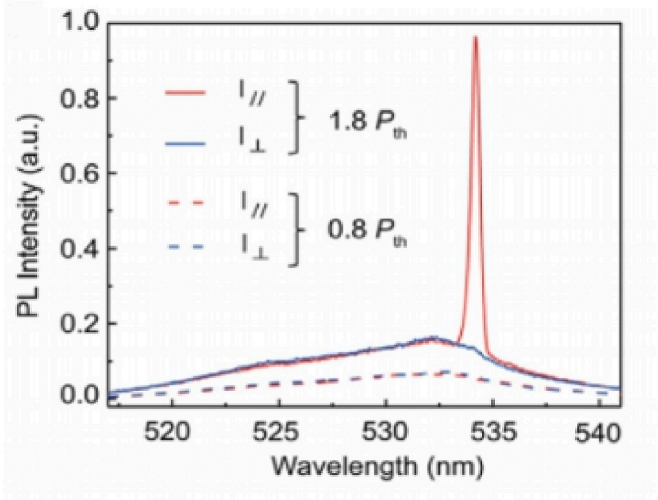

Fig. 17. PL spectroscopy of perovskite microcavity. The P_{th} is power threshold about $3.5\mu Jcm^{-2}$. The red/blue curve is parallel/perpendicular to the linear polarization direction. This picture is adapted from reference [52]. (For interpretation of the references to colour in this figure legend, the reader is referred to the Web version of this article.)

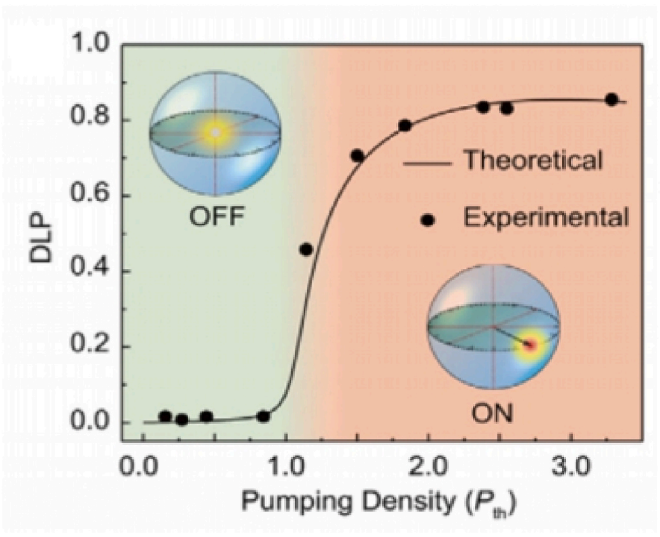

Fig. 18. Diagram of DLP switch. This picture is adapted from reference [52].

3.2. Terahertz binary all-optical encoder based on DLP switch

The value of DLP is related to the wavelength, polarization and power intensity of the excitation source. Therefore, the "0″ and "1″ of DLP are controlled by changing the excitation source parameters.

The high DLP (DLP>0.6) has the same order of about 10 ps as the duration of the laser process, see Fig. 19. By controlling the excitation moments and excitation power to generate multiple PL short pulses, write perovskite micro-encoders according to your own expectations, as shown in the Fig. 20:

Define the average value of DLP compared with 0.6 to design digital signals "0" and "1". The bandwidth of the DLP encoder is adjustable with an upper limit of 0.1 THz, which is determined by the laser duration of the perovskite microstructure. In addition, the interval between each set of encoded information needs to be taken into account.

3.3. Multi-layer coding

We can see that the radiation source type encoder is achieved by changing the excitation parameters from the design principle of the DLP encoder of section 3.2. If we want to achieve high-order encoder, we also need other laser source or other parameters caused by laser control (intensity, polarization, pulse shape, etc.) as additional coding information. There are two high-order coding methods here. One is to add additional excitation sources to supplement other relevant parameters of the excitation as coding information. The second is to control other mutation parameters of the excitation source as supplementary coding information. Here introduces a ternary encoder by adding an additional excitation source. The additional pump pulse beam is 800 nm wavelength, used for shape parameter coding [121–123]. There will be obvious two-photon absorption phenomenon between the high power 800 nm pump pulse and the MS perovskite, as shown in Fig. 21.

Fig. 21 can see when the pump pulse is greater than $50\mu Jcm^{-2}$ two-photon absorption is obvious; the shape coding feature information is effective. Since two-photon absorption involves dynamic carrier relaxation within the material, an effective delay of 5–10 ps is applied to the 800 nm beam in order to effectively adjust the shape between the two pump pulses, as shown in Fig. 22.

The effective delay makes the two encoding parameters of DLP and pulse shape in the smallest common period, so that the encoding period of the new encoding method is the shortest. The combination of DLP encoding parameters and pulse shape parameters forms a new marking state "2" and realizes the conversion from binary to ternary. Here we also define a coding principle for the fourth state "3", based on the

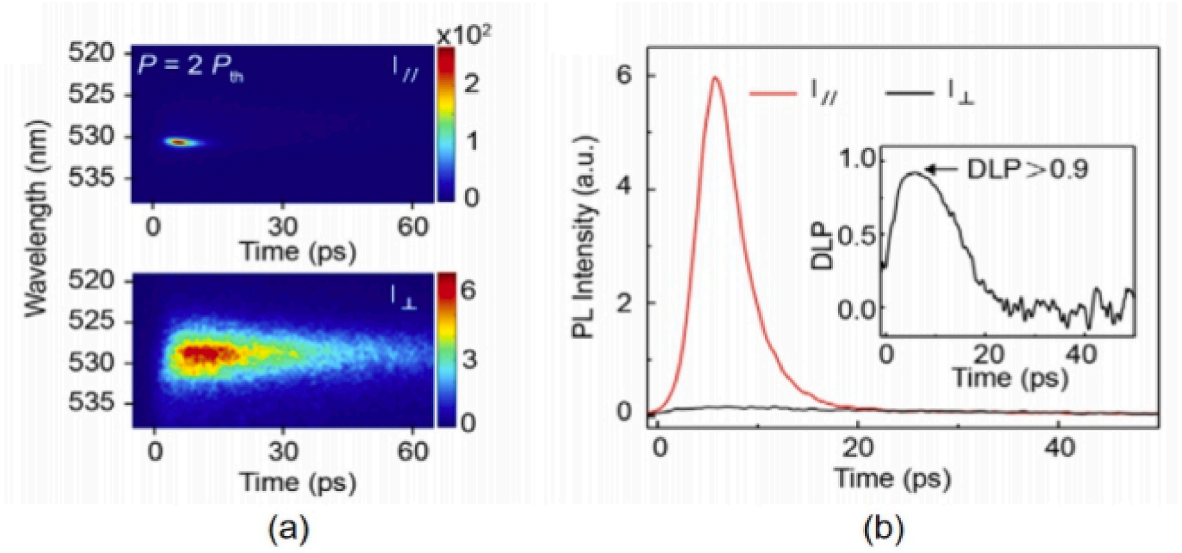

Fig. 19. (a) Polarized PL dynamics (b) Linearly polarized PL spectra of $I_{\parallel}$ (Red lines) and $I_{\perp}$ (Blackline). Inset: DLP dynamics. This picture is adapted from reference [52]. (For interpretation of the references to colour in this figure legend, the reader is referred to the Web version of this article.)

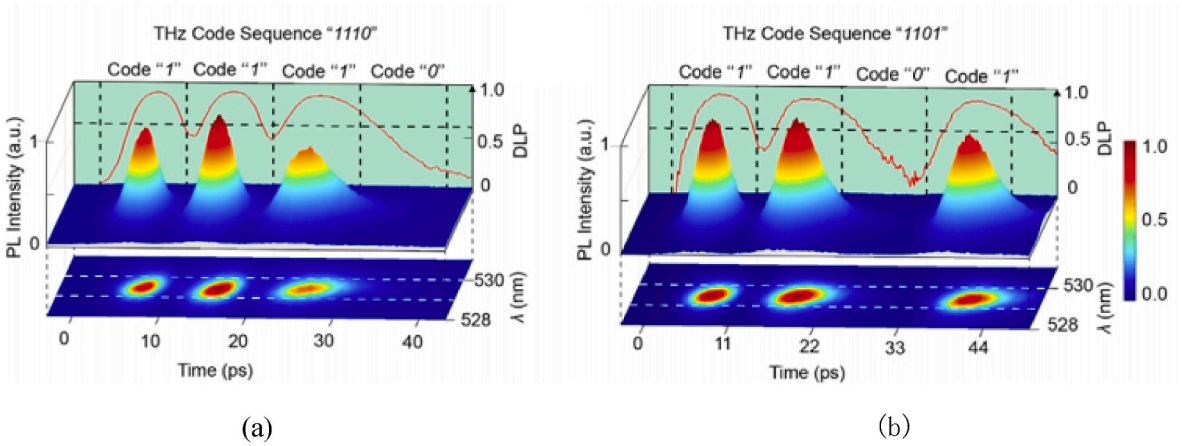

Fig. 20. (a) Schematic diagram of using DLP coding "1110" achieve 0.1 THz bandwidth (b) THz Code Sequence "1101" using DLP encoding. This picture is adapted from reference [52].

above-mentioned ternary. The fourth state is "two-photon absorption exist but low DLP".

4. Conclusions

All-optical encoder is an information conversion logic device that only uses light as an information carrier, and can solve the speed bottleneck caused by the photoelectric conversion delay of the traditional optical encoder. The low influence between photons compared with electrons can effectively reduce the interference of the surrounding electromagnetic field, and has a high coding accuracy. With the development of semiconductor integration technology, the requirements for miniaturization of smart equipment have become higher. As an important device in the field of information conversion, all-optical encoders have been widely used in many aspects. Therefore, the main development direction of all-optical encoders is miniaturized design on the basis of not reducing the encoding speed. With the vigorous development of communication technology, 5G communication has driven the development of many ultra-fast fields such as artificial intelligence, remote control, aerospace communication, etc. As a new generation of encoding devices, all-optical encoders can effectively meet the integration of equipment matching and information transmission function.

In this review, we describe the latest design methods for all-optical encoders, and explore various optimization angles for size, material and application matching. All-optical encoders are divided into two major categories. One is the design of defect encoders based on 2D PhCs, which effectively utilizes the interaction of light beams and PhCs to design the light propagation path. Then, the design principles are divided into three steps: propagation, control, and optimization. Propagation is mainly designed by self-collimation effect or line defect waveguide. Control is mainly realized by the ring resonator blocking effect or the reflector and beamsplitter designed by line defect. The optimization part is based on the radius control and position control of point defects to improve output efficiency and reduce energy loss. The switching state of the linear 2D PhC all-optical encoder is defined by the lasing regime or the non-lasing case. It is not necessary to use a high-intensity pump pulse and a nonlinear Kerr effect to form an optical switch like a nonlinear crystal.

The second type of all-optical encoder is based on radiation source parameter control. This type of encoder is currently poorly understood, but it can further break the size limit of 2D PhC. Therefore, it has important application prospects in the future of ultra-fast information

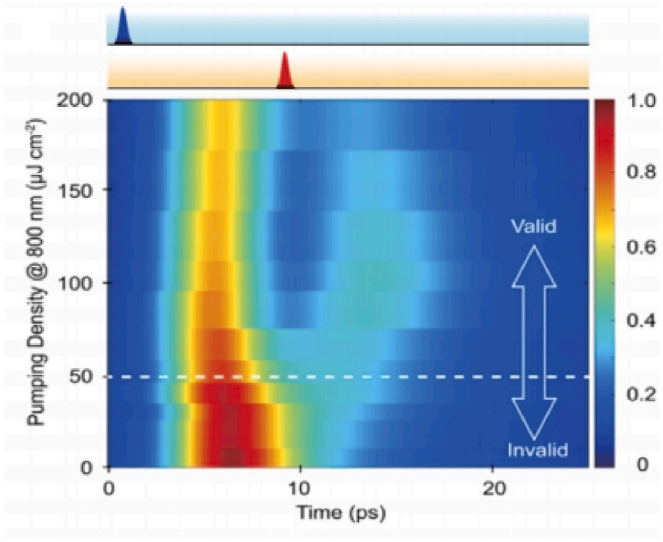

Fig. 21. Diagram of effective two-photon absorption area distribution. This picture is adapted from reference [52].

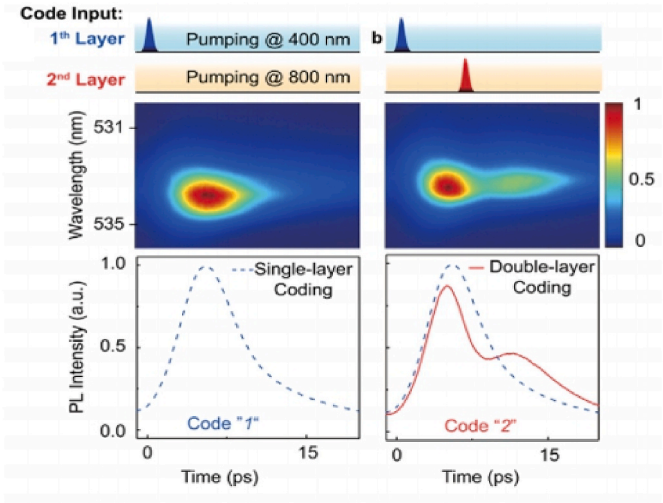

Fig. 22. The shape of pulse encoding with 5–10 ps delay under double layer. This picture is adapted from reference [52].

coding. A series of instantaneous changes in optical parameters such as energy, waveform, polarization, frequency, wavelength, etc. can be encoded as optical switches. For achieving high-order coding, people can add additional excitation sources to participate in multi-layer control.

Author statement

All the contents of this paper are jointly completed by the author Debao Zhang and Guanjun You. Debao Zhang mainly completed the literature investigation and writing, and discussed the content of the article with Guanjun You. There is no conflict of interest between authors.

Declaration of competing interest

The authors declare that they have no known competing financial interests or personal relationships that could have appeared to influence the work reported in this paper.

Acknowledgments

This work is supported by the National Key Research and Development Program of China 2016YFF0200306 and 2017YFF0106304.

Appendix A. Supplementary data

Supplementary data to this article can be found online at https://doi.org/10.1016/j.physe.2020.114469.

References

[1] Xianyu Li, et al., The integration technology and analysis of information system, Appl. Mech. Mater. 263–266 (Dec.2012), https://doi.org/10.4028/www.scientific.net/amm.263-266.1242.
[2] Y. Yang, Y. Yamagami, X. Yu, et al., Terahertz topological photonics for on-chip communication, Nat. Photon. (2020), https://doi.org/10.1038/s41566-020-0618-9.
[3] Genwang Wang, H.O.U. Chaojian, L.O.N.G. Haotian, Y.A.N.G. Lijun, W.A.N. G. Yang, Electronic and optoelectronic nanodevices based on two-dimensional semiconductor materials [J], Acta Phys. Chim. Sin. 35 (12) (2019) 1319–1340, https://doi.org/10.3866/PKU.WHXB201903010.
[4] H. Elayan, O. Amin, B. Shihada, R.M. Shubair, M. Alouini, Terahertz band: the last piece of RF spectrum puzzle for communication systems, IEEE Open J. Commun. Soc. 1 (2020) 1–32, https://doi.org/10.1109/OJCOMS.2019.2953633.
[5] Y. Yang, Y. Yamagami, X. Yu, et al., Terahertz topological photonics for on-chip communication, Nat. Photon. (2020), https://doi.org/10.1038/s41566-020-0618-9.
[6] Il-Pyeong Hwang, Chang-Hee Lee, A perfect secure optical-network with an anti-correlated noise, Optic Commun. 466 (2020), https://doi.org/10.1016/j.optcom.2020.125649, 125649,ISSN 0030-4018.
[7] H.Z. Zhou, S.F. Liu, X.C. Kang, N. Zhu, K.L. Lv, Y.M. Zhang, S.L. Pan, Broadband two-thirds photonic microwave frequency divider, Electron. Lett. 55 (21) (2019) 1141–1143, https://doi.org/10.1049/el.2019.2159.
[8] Y. Xu, et al., Injection-locked millimeter wave frequency divider utilizing optoelectronic oscillator based optical frequency comb, IEEE Photon. J. 11 (3) (2019) 1–8, https://doi.org/10.1109/JPHOT.2019.2916919. Art no. 5501508.
[9] A.Y. Zherdev, S.B. Odinokov, M.S. Kovalev, D.S. Lushnikov, V.V. Markin, M. V. Shishova, N.G. Stsepuro, Investigation of structured head diffraction gratings for linear optical encoder, in: Proc. SPIE 10818, Holography, Diffractive Optics, and Applications, vol. vol. III, 2018, p. 108181B, https://doi.org/10.1117/12.2326998.
[10] Y. Vázquez-Gutiérrez, D.L. O'Sullivan, R.C. Kavanagh, Small-signal modeling of the incremental optical encoder for motor control, IEEE Trans. Ind. Electron. 67 (5) (May 2020) 3452–3461, https://doi.org/10.1109/TIE.2019.2916307.
[11] Jili Deng, Xiaona Yan, Chunlong Wei, Yangcong Lu, Mingkang Li, Xiansong Xiang, Wei Jia, Changhe Zhou, Eightfold optical encoder with high-density grating, Appl. Optic. 57 (2018) 2366–2375, https://doi.org/10.1364/AO.57.002366.
[12] Anuj Kumar Sharma, Sandeep Sharma, Santosh Kumar, Design and analysis of an optical FIR filter, in: Proc. SPIE 9889, Optical Modelling and Design, vol. IV, 27 April 2016, p. 98892A, https://doi.org/10.1117/12.2231022.
[13] Z. Ren, Y. Sun, J. Hu, S. Zhang, Z. Lin, X. Zhi, Electro-optic filter based on guided-mode resonance for optical communication, Electron. Lett. 54 (23) (15 11 2018) 1340–1342, https://doi.org/10.1049/el.2018.5034.
[14] C. Bolle, A. Sridhar, H. Safar, D. Neilson, M. Cappuzzo, M. Earnshaw, A fast and low-loss electromagnetically tunable optical filter, IEEE Photon. Technol. Lett. 30 (9) (2018) 837–840, https://doi.org/10.1109/LPT.2018.2819885, 1 May1.
[15] F. Mehdizadeh, M. Soroosh, H. Alipour-Banaei, A novel proposal for optical decoder switch based on photonic crystal ring resonators, Opt. Quant. Electron. 48 (2016) 20, https://doi.org/10.1007/s11082-015-0313-0.
[16] Farhad Mehdizadeh, Hamed Alipour-Banaei, Somaye Serajmohammadi, Study the role of non-linear resonant cavities in photonic crystal-based decoder switches, J. Mod. Optic. 64 (13) (2017) 1233–1239, https://doi.org/10.1080/09500340.2016.1275854.
[17] S.S. Zamanian-Dehkordi, M. Soroosh, G. Akbarizadeh, An ultra-fast all-optical RS flip-flop based on nonlinear photonic crystal structures, Opt. Rev. 25 (2018) 523–531, https://doi.org/10.1007/s10043-018-0443-2.
[18] M.J. Maleki, A. Mir, M. Soroosh, Designing an ultra-fast all-optical full-adder based on nonlinear photonic crystal cavities, Opt. Quant. Electron. 52 (2020) 196, https://doi.org/10.1007/s11082-020-02311-x.
[19] S. Swarnakar, S. Kumar, S. Sharma, Performance analysis of all-optical full-adder based on two-dimensional photonic crystals, J. Comput. Electron. 17 (2018) 1124–1134, https://doi.org/10.1007/s10825-018-1177-x.
[20] HuGe Jile, Realization of an all-optical comparator using beam interference inside photonic crystal waveguides, Appl. Optic. 59 (2020) 3714–3719, https://doi.org/10.1364/AO.385744.
[21] Seraj Zahra, Mohammad Soroosh, Navid Alaei-Sheini, Ultra-compact ultra-fast 1-bit comparator based on a two-dimensional nonlinear photonic crystal structure, Appl. Optic. 59 (2020) 811–816, https://doi.org/10.1364/AO.374428.

[22] T. Ahmadi Tameh, M. Sawan, R. Kashyap, Novel analog ratio-metric optical rotary encoder for avionic applications, IEEE Sensor. J. 16 (17) (2016) 6586–6595, https://doi.org/10.1109/JSEN.2016.2588981. Sept.1.
[23] W. Bahn, J. Nam, S. Lee, D.D. Cho, Digital optoelectrical pulse method for vernier-type rotary encoders, IEEE Trans. Instrum. Meas. 65 (2) (Feb. 2016) 431–440, https://doi.org/10.1109/TIM.2015.2502878.
[24] Subir Das, Tuhin Subhra Sarkar, Badal Chakraborty, Himadri Sekhar Dutta, Study on array of photo-detector based absolute rotary encoder, Sensor Actuator Phys. 246 (2016) 114–122, https://doi.org/10.1016/j.sna.2016.05.026. ISSN 0924-4247.
[25] J. Jovanovic, D. Denic, U. Jovanovic, An improved linearization circuit used for optical rotary encoders, Meas. Sci. Rev. 17 (5) (2017) 241–249, https://doi.org/10.1515/msr-2017-0029.
[26] Mahdi Hassangholizadeh-Kashtiban, Reza Sabbaghi-Nadooshan, Hamed Alipour-Banaei, A novel all optical reversible 4×2 encoder based on photonic crystals, Optik 126 (20) (2015) 2368–2372, https://doi.org/10.1016/j.ijleo.2015.05.140. ISSN 0030-4026.
[27] Yang Wang, Xinliang Zhang, Jianji Dong, Dexiu Huang, Simultaneous demonstration on all-optical digital encoder and comparator at 40 Gb/s with semiconductor optical amplifiers, Optic Express 15 (2007) 15080–15085, https://doi.org/10.1364/OE.15.015080.
[28] T. Chattopadhyay, J.N. Roy, An all-optical technique for a binary-to-quaternary encoder and a quaternary-to-binary decoder, J. Optic. Pure Appl. Optic. 11 (7) (2009) 8, https://doi.org/10.1088/1464-4258/11/7/075501.
[29] Purnima Sethi, Sukhdev Roy, All-optical ultrafast XOR/XNOR logic gates, binary counter, and double-bit comparator with silicon microring resonators, Appl. Optic. 53 (2014) 6527–6536, https://doi.org/10.1364/AO.53.006527.
[30] H. Soto, A. Gutiérrez, All-optical 2-to-4 level encoder based on cross polarization modulation in a semiconductor optical amplifier utilized to develop an all-optical 2 input digital multiplexer, Optic Express 14 (2006) 9000–9005, https://doi.org/10.1364/OE.14.009000.
[31] Weidong Zhou, Deyin Zhao, Yi-Chen Shuai, Hongjun Yang, Santhad Chuwongin, Arvinder Chadha, Jung-Hun Seo, Ken X. Wang, Victor Liu, Zhenqiang Ma, Shanhui Fan, Progress in 2D photonic crystal Fano resonance photonics, Prog. Quant. Electron. 38 (Issue 1) (2014), https://doi.org/10.1016/j.pquantelec.2014.01.001.
[32] L. Lu, C. Fang, L. Fu, et al., Symmetry-protected topological photonic crystal in three dimensions, Nat. Phys. 12 (2016) 337–340, https://doi.org/10.1038/nphys3611.
[33] A. Arie, N. Voloch, Periodic, quasi-periodic, and random quadratic nonlinear photonic crystals, Laser Photon. Rev. 4 (3) (2010) 355–373, https://doi.org/10.1002/lpor.200910006.
[34] Youngsuk Nam, Yi Xiang Yeng, Andrej Lenert, Peter Bermel, Ivan Celanovic, Marin Soljačić, Evelyn N. Wang, Solar thermophotovoltaic energy conversion systems with two-dimensional tantalum photonic crystal absorbers and emitters, Sol. Energy Mater. Sol. Cell. 122 (2014), https://doi.org/10.1016/j.solmat.2013.12.012.
[35] Mahmoud Youcef Mahmoud, Ghaouti Bassou, Taalbi Ahmed, Zoheir Mohamed Chekroun, Optical channel drop filters based on photonic crystal ring resonators, Optic Commun. 285 (Issue 3) (2012), https://doi.org/10.1016/j.optcom.2011.09.068.
[36] J.B. Chou, et al., Enabling ideal selective solar absorption with 2D metallic dielectric photonic crystals, Adv. Mater. 26 (47) (2014) 8041–8045, https://doi.org/10.1002/adma.201403302.
[37] Xue Quan, Kam Man Shum, Chi Hou Chan, Novel 1-D microstrip PBG cells, IEEE Microw. Guid. Wave Lett. 10 (10) (Oct. 2000) 403–405, https://doi.org/10.1109/75.877226.
[38] Kam Man Shum, Xue Quan, Chi Hou Chan, A novel microstrip ring hybrid incorporating a PBG cell, IEEE Microw. Wireless Compon. Lett. 11 (6) (June 2001) 258–260, https://doi.org/10.1109/7260.928931.
[39] W. Barnes, A. Dereux, T. Ebbesen, Surface plasmon subwavelength optics, Nature 424 (2003) 824–830, https://doi.org/10.1038/nature01937.
[40] C. López, Materials aspects of photonic crystals, Adv. Mater. 15 (2003) 1679–1704, https://doi.org/10.1002/adma.200300386.
[41] Iman Ouahab, Rafah Naoum, A novel all optical 4×2 encoder switch based on photonic crystal ring resonators, Optik 127 (Issue 19) (2016), https://doi.org/10.1016/j.ijleo.2016.05.080.
[42] Amir Salimzadeh, Hamed Alipour-Banaei, An all optical 8 to 3 encoder based on photonic crystal OR-gate ring resonators, Optic Commun. 410 (2018), https://doi.org/10.1016/j.optcom.2017.11.036.
[43] Farhad Mehdizadeh, Hamed Alipour-Banaei, Somaye Serajmohammadi, Design and simulation of all optical decoder based on nonlinear PhCRRs, Optik 156 (2018), https://doi.org/10.1016/j.ijleo.2017.12.011.
[44] A. Tamer, Moniem. All-Optical XNOR Gate Based on 2D Photonic-Crystal Ring Resonators, March 2017, https://doi.org/10.1070/QEL16279.
[45] Yi-Pin Yang, Kuen-Cherng Lin, I-Chen Yang, Kun-Yi Lee, Wei-Yu Lee, Yao-Tsung Tsai, All-optical photonic-crystal encoder capable of operating at multiple wavelengths, Optik 142 (2017), https://doi.org/10.1016/j.ijleo.2017.05.067.
[46] Li Liu, Jianji Dong, Xinliang Zhang, Chip-integrated all-optical 4-bit Gray code generation based on silicon microring resonators, Optic Express 23 (2015) 21414–21423, https://doi.org/10.1364/OE.23.021414.
[47] M.R. Jalali-Azizpoor, M. Soroosh, Y. Seifi-Kavian, Application of self-collimated beams in realizing all-optical photonic crystal-based half-adder, Photonic Netw. Commun. 36 (2018) 344–349, https://doi.org/10.1007/s11107-018-0786-4.
[48] E.G. Anagha, A. Rajesh, D. Saranya, Design of an all optical encoder using 2D photonic crystals, in: PROCEEDINGS OF THE 2ND INTERNATIONAL CONFERENCE ON INVENTIVE SYSTEMS AND CONTROL, 2018.
[49] Mohebzadeh-Bahabady Ahmad, Saeed Olyaee, Designing an ultracompact all-optical 4-to-2 encoder and investigating its optical power consumption, Appl. Optic. 59 (2020) 2409–2415, https://doi.org/10.1364/AO.381780.
[50] S. Monisha, D. Saranya, A. Rajesh, Design and analysis of multi-hexagonal reversible encoder using photonic crystals, Opt. Quant. Electron. 51 (2019) 6, https://doi.org/10.1007/s11082-018-1718-3.
[51] A. Chabanov, M. Stoytchev, A. Genack, Statistical signatures of photon localization, Nature 404 (2000) 850–853, https://doi.org/10.1038/35009055.
[52] Y. Zhong, B. Tang, M. Fei, Q. Jie, J. Tan, Q. Wang, S. Liang, J. Du, L. Zhang, H. Dong, W. Xie, All-photonic miniature perovskite encoder with a terahertz bandwidth, Laser Photon. Rev. 14 (2020) 1900398, https://doi.org/10.1002/lpor.201900398.
[53] H. Zhang, X. Wang, Q. Liao, Z. Xu, H. Li, L. Zheng, H. Fu, Embedding perovskite nanocrystals into a polymer matrix for tunable luminescence probes in cell imaging, Adv. Funct. Mater. 27 (2017) 1604382, https://doi.org/10.1002/adfm.201604382.
[54] Chao-Yang Lu, Wei-Bo Gao, Jin Zhang, Xiao-Qi Zhou, Tao Yang, Jian-Wei Pan, Experimental quantum coding against qubit loss error, Proc. Natl. Acad. Sci. U.S.A. 105 (32) (2008) 11050–11054, https://doi.org/10.1073/pnas.0800740105.
[55] S. Stranks, H. Snaith, Metal-halide perovskites for photovoltaic and light-emitting devices, Nat. Nanotechnol. 10 (2015) 391–402, https://doi.org/10.1038/nnano.
[56] J. Song, J. Li, X. Li, L. Xu, Y. Dong, H. Zeng, Quantum dot light-emitting diodes based on inorganic perovskite cesium lead halides (CsPbX3), Adv. Mater. 27 (2015) 7162–7167, https://doi.org/10.1002/adma.201502567.
[57] Gopal K. Mor, Oomman K. Varghese, Maggie Paulose, Karthik Shankar, Craig A. Grimes, A review on highly ordered, vertically oriented TiO2 nanotube arrays: fabrication, material properties, and solar energy applications, Sol. Energy Mater. Sol. Cell. 90 (Issue 14) (2006), https://doi.org/10.1016/j.solmat.2006.04.007.
[58] Richard W. Ziolkowski, Ehud Heyman, Wave propagation in media having negative permittivity and permeability, Phys. Rev. E 64 (2001), 056625, https://doi.org/10.1103/PhysRevE.64.056625.
[59] Alexandre Vial, Anne-Sophie Grimault, Demetrio Macías, Dominique Barchiesi, Marc Lamy de la Chapelle, Improved analytical fit of gold dispersion: application to the modeling of extinction spectra with a finite-difference time-domain method, Phys. Rev. B 71 (2005), 085416, https://doi.org/10.1103/PhysRevB.71.085416.
[60] Fenghua Zhen, Zhizhang Chen, Jiazong Zhang, Toward the development of a three-dimensional unconditionally stable finite-difference time-domain method, IEEE Trans. Microw. Theor. Tech. 48 (9) (Sept. 2000) 1550–1558, https://doi.org/10.1109/22.869007.
[61] D. Hillerkuss, R. Schmogrow, T. Schellinger, et al., 26 Tbit s−1 line-rate super-channel transmission utilizing all-optical fast Fourier transform processing, Nat. Photon. 5 (2011) 364–371, https://doi.org/10.1038/nphoton.2011.74.
[62] Leslie Greengard, June-Yub Lee, Accelerating the nonuniform fast fourier transform, SIAM (Soc. Ind. Appl. Math.) Rev. 46 (3) (2004) 443–454, https://doi.org/10.1137/S003614450343200X.
[63] Kazutaka Katoh, Kazuharu Misawa, Kei-ichi Kuma, Takashi Miyata, MAFFT: a novel method for rapid multiple sequence alignment based on fast Fourier transform, Nucleic Acids Res. 30 (Issue 14) (15 July 2002) 3059–3066, https://doi.org/10.1093/nar/gkf436.
[64] I.V. Guryev, I.A. Sukhoivanov, Plane Wave Expansion Method with Considered Material Dispersion, The Experience of Designing and Applications of CAD Systems in Microelectronics, Lviv-Polyana, 2007, https://doi.org/10.1109/CADSM.2007.4297472.
[65] B.K. Shukla, R.H. Patel, Simulation of paraxial beam propagation using plane wave expansion method, in: 2008 International Conference on Recent Advances in Microwave Theory and Applications, Jaipur, 2008, pp. 652–656, https://doi.org/10.1109/AMTA.2008.4763220.
[66] Vivek Krishnamurthy, Benjamin Klein, Comprehensive theory of plane-wave expansion based eigenmode method for scattering-matrix analysis of photonic structures, J. Opt. Soc. Am. B 26 (2009) 1341–1350, https://doi.org/10.1364/JOSAB.26.001341.
[67] Zhu Xue-Feng1, Liu Sheng-Chun2, Tao1 Xu, Tie-Hai1 Wang, Cheng Jian-Chun1, Investigation of a silicon-based one-dimensional phononic crystal plate via the super-cell plane wave expansion method, Chin. Phys. B (2010), https://doi.org/10.1088/1674-1056/19/4/044301.
[68] Y. Zhu, Y. Zhuang, X. Shi, An improved algorithm of photonic crystal fibers' defect mode based on the plane-wave expansion and supercell method, in: 2014 International Symposium on Computer, Consumer and Control, Taichung, 2014, pp. 322–325, https://doi.org/10.1109/IS3C.2014.91.
[69] H.T. Zhang, D.S. Wang, M.L. Gong, D.Z. Zhao, Application of group theory to plane wave expansion method for photonic crystals, Optic Commun., Volume 237, **2004**; doi:10.1016/j.optcom.2004.03.075.
[70] Mahmoud I. Hussein, Gregory M. Hulbert, Mode-enriched dispersion models of periodic materials within a multiscale mixed finite element framework, Finite Elem. Anal. Des. (2006), https://doi.org/10.1016/j.finel.2005.11.002.
[71] S.A. Mallios, G.P. Latsas, I.G. Tigelis, TE waves in arbitrary periodic slow-wave structures with rectangular grooves, J. Infrared, Millim. Terahertz Waves 30 (2009) 1113–1122, https://doi.org/10.1007/s10762-009-9532-4.
[72] I.G. Tigelis, J. Raguin, Z.C. Ioannidis, et al., Dispersion characteristics of arbitrary periodic structures with rectangular grooves, Int. J. Infrared Millimet. Waves 29 (2008) 432–442, https://doi.org/10.1007/s10762-008-9338-9.

[73] S.M. Rudolph, A. Grbic, The design of broadband, volumetric NRI media using multiconductor transmission-line analysis, IEEE Trans. Antenn. Propag. 58 (4) (April 2010) 1144–1154, https://doi.org/10.1109/TAP.2010.2041314.
[74] Yuanliang Zhang, Yao Zhang, Baojun Li, Optical switches and logic gates based on self-collimated beams in two-dimensional photonic crystals, Optic Express 15 (2007) 9287–9292, https://doi.org/10.1364/OE.15.009287.
[75] Hamed Alipour-Banaei, Mehdi Ghorbanzadeh Rabati, Parisa Abdollahzadeh-Badelbou, Farhad Mehdizadeh, Application of self-collimated beams to realization of all optical photonic crystal encoder, Phys. E Low-dimens. Syst. Nanostruct. (2016), https://doi.org/10.1016/j.physe.2015.08.011.
[76] H. Kosaka, T. Kawashima, A. Tomita, M. Notomi, T. Tamamura, T. Sato, S. Kawakami, Self-collimating phenomena in photonic crystals,, Appl. Phys. Lett. 74 (1999) 1212–1214, https://doi.org/10.1063/1.123502.
[77] J. Witzens, M. Lonn ar, A. Scherer, Self-collimation in planar photonic crystals, IEEE J. Sel. Top. Quant. Electron. 8 (2002) 1246–1257, https://doi.org/10.1109/JSTQE.2002.806693.
[78] X. Yu, S. Fan, Bends and splitters for self-collimated beams in photonic crystals, Appl. Phys. Lett. 833251–3253 (2003), https://doi.org/10.1063/1.1621736.
[79] S.-G. Lee, S.S. Oh, J.-E. Kim, H.Y. Park, C.-S. Kee, Line-defect-induced bending and splitting of self-collimated beams in two-dimensional photonic crystals, Appl. Phys. Lett. 87 (2005) 1811061–1811063, https://doi.org/10.1063/1.2112186.
[80] M.-W. Kim, S.-G. Lee, T.T. Kim, J.E. Kim, H.Y. Park, C.-S. Kee, Experimental demonstration of bending and splitting of self-collimated beams in two-dimensional photonic crystals, Appl. Phys. Lett. 90 (2007), 1131211-3, https://doi.org/10.1063/1.2713859.
[81] C. Chen, A. Sharkawy, D.M. Pustai, S. Shi, D.W. Prather, Optimizing bending efficiency of self-collimated beams in non-channel planar photonic crystal waveguides, Optic Express 11 (2003) 3153–3159, https://doi.org/10.1364/OE.11.003153.
[82] B. Miao, C. Chen, S. Shi, D.W. Prather, A high-efficiency in-plane splitting coupler for planar photonic crystal self-collimation devices, IEEE Photon. Technol. Lett. 17 (2005) 61–63, https://doi.org/10.1109/LPT.2004.838138.
[83] M. Noori, M. Soroosh, H. Baghban, Self-collimation in photonic crystals: applications and opportunities, Ann. Phys. (2018), https://doi.org/10.1002/andp.201700049.
[84] Mina Noori, Mohammad Soroosh, Hamed Baghban, Design of highly efficient polarization beam splitter based on self-collimation on Si platform, J. Mod. Optic. 64 (5) (2017) 491–499, https://doi.org/10.1080/09500340.2016.1244294.
[85] M. Slabs, K. Notomi, A. Yamada, J. Shinya, C. Takahashi Takahashi, I. Yokohama, Extremely large group-velocity dispersion of line-defect waveguides in photonic crystal, Phys. Rev. Lett. 87 (2001) 253902, https://doi.org/10.1103/PhysRevLett.87.253902.
[86] Eiichi Kuramochia, Masaya Notomi, Satoshi Mitsugi, Akihiko Shinya, Takasumi Tanabe, Ultrahigh-QQ photonic crystal nanocavities realized by the local width modulation of a line defect, Appl. Phys. Lett. 88 (2006), 041112, https://doi.org/10.1063/1.2167801.
[87] Masatoshi Tokushima, Hideo Kosaka, Akihisa Tomita, Hirohito Yamada, Lightwave propagation through a 120° sharply bent single-line-defect photonic crystal waveguide, Appl. Phys. Lett. 76 (2000) 952, https://doi.org/10.1063/1.125902.
[88] M. Notomi, A. Shinya, K. Yamada, J.- Takahashi, C. Takahashi, I. Yokohama, Structural tuning of guiding modes of line-defect waveguides of silicon-on-insulator photonic crystal slabs, IEEE J. Quant. Electron. 38 (7) (July 2002) 736–742, https://doi.org/10.1109/JQE.2002.1017583.
[89] Yoshimasa Sugimoto, Tanaka Yu, Naoki Ikeda, Yusui Nakamura, Kiyoshi Asakawa, Kuon Inoue, Low propagation loss of 0.76 dB/mm in GaAs-based single-line-defect two-dimensional photonic crystal slab waveguides up to 1 cm in length, Optic Express 12 (2004) 1090–1096, https://doi.org/10.1364/OPEX.12.001090.
[90] N. Malkova, C.Z. Ning, Phys. Light propagation through a sharp-bend coupled-cavity waveguide in a two-dimensional photonic crystal, Phys. Rev. B 73 (2006) 155101, https://doi.org/10.1103/PhysRevB.73.155101.
[91] N. Malkova, C.-Z. Ning, V. Gopalan, Resonant light propagation through 90deg bend waveguide based on strained two-dimensional photonic crystal, IEEE Cat (4TH8728) (2004).
[92] Hirohito Yamada, Tao Chu, Akiko Gomyo, Jun Ushida, Masayuki Shirane, Satomi Ishida, Yasuhiko Arakawa, Photonic Crystal Slab and Si-Wire Waveguide Devices, 2004, https://doi.org/10.1117/12.690987.
[93] Danny Eliyahu, Lev S. Sadovnik, Vladimir A. Manasson, Millimeter-wave waveguiding using photonic band structures, in: Enabling Photonic Technologies for Aerospace Applications II, vol. 4042, 2000, https://doi.org/10.1117/12.391908. Author Affiliations Proceedings.
[94] Farhad Mehdizadeh, Mohammad Soroosh, Hamed Alipour-Banaei, Proposal for 4-to-2 optical encoder based on photonic crystals, IET Optoelectron. 11 (1) (2017) 29–35, https://doi.org/10.1049/iet-opt.2016.0022.
[95] Ahmad Mohebzadeh-Bahabady, Saeed Olyaee, All-optical NOT and XOR logic gates using photonic crystal nano-resonator and based on an interference effect, IET Optoelectron. 12 (4) (2018) 191–195, https://doi.org/10.1049/iet-opt.2017.0174.
[96] Fariborz Parandin, High contrast ratio all-optical 4 × 2 encoder based on two-dimensional photonic crystals, Optic Laser. Technol. 113 (2019), https://doi.org/10.1016/j.optlastec.2019.01.003.
[97] Y. Yuan Wang, Performance research of photonic crystal micro-cavity, in: CNKI, Chinese, 2009.
[98] S. Gholamnejad, M. Zavvari, Design and analysis of all-optical 4–2 binary encoder based on photonic crystal, Opt. Quant. Electron. 49 (2017) 302, https://doi.org/10.1007/s11082-017-1144-y.
[99] J.K. Jayabarathan, G. Subhalakshmi, S. Robinson, Design of all-optical 8*3 encoder using hexagonal shaped photonic crystal ring resonator, J. Ovonic Res. 14 (2018) 351–358.
[100] Hongxing Zhang, wei Pan, Xinkai Liu, Study on Ring Resonator Characteristics of Photonic Crystals, STUDY ON OPTICAL COMMUNICATIONS, Chinese, 2011.
[101] A. Tamer, Moniem, All-optical digital 4 × 2 encoder based on 2D photonic crystal ring resonators, J. Mod. Optic. 63 (8) (2016) 735–741, https://doi.org/10.1080/09500340.2015.1094580.
[102] T.S. Mostafa, N.A. Mohammed, E.M. El-Rabaie, Ultracompact ultrafast-switching-speed all-optical 4 × 2 encoder based on photonic crystal, J. Comput. Electron. 18 (2019) 279–292, https://doi.org/10.1007/s10825-018-1278-6.
[103] F. Haddadan, M. Soroosh, Low-power all-optical 8-to-3 encoder using photonic crystal-based waveguides, Photonic Netw. Commun. 37 (2019) 83–89, https://doi.org/10.1007/s11107-018-0795-3.
[104] Amir Salimzadeh, Hamed Alipour-Banaei, An all optical 8 to 3 encoder based on photonic crystal OR-gate ring resonators, Optic Commun. (2018), https://doi.org/10.1016/j.optcom.2017.11.036.
[105] Fatemeh Haddadan, Mohammad Soroosh, Navid Alaei-Sheini, Designing an electro-optical encoder based on photonic crystals using the graphene–Al_2O_3 stacks, Appl. Optic. 59 (2020) 2179–2185, https://doi.org/10.1364/AO.386248.
[106] Mohebzadeh-Bahabady Ahmad, Saeed Olyaee, Designing an ultracompact all-optical 4-to-2 encoder and investigating its optical power consumption, Appl. Optic. 59 (2020) 2409–2415, https://doi.org/10.1364/AO.381780.
[107] M. Qiu, K. Azizi, A. Karlsson, M. Swillo, B. Jaskorzynska, Numerical studies of mode gaps and coupling efficiency for line-defect waveguides in two-dimensional photonic crystals, Phys. Rev. B 64 (2001) 155113, https://doi.org/10.1103/PhysRevB.64.155113.
[108] Min Qiu, Effective index method for heterostructure-slab-waveguide-based two-dimensional photonic crystals, Appl. Phys. Lett. 81 (2002) 1163, https://doi.org/10.1063/1.1500774.
[109] Fatemeh Hadadan1, Mohammad Soroosh, A new proposal for 4-to-2 optical encoder using nonlinear photonic crystal ring resonators, Int. J. Ophthalmic. Pract. (2019), https://doi.org/10.29252/ijop.13.2.119.
[110] Z.-H. Zhu, W.-M. Ye, J.-R. Ji, X.-D. Yuan, C. Zen, High-contrast light-by-light switching and AND gate based on nonlinear photonic crystals, Opt.Express 14 (2006) 1783–1788, https://doi.org/10.1364/OE.14.001783.
[111] H. Azuma, Quantum computation with Kerr-nonlinear photonic crystals, J. Phys. D Appl. Phys. 41 (2008) 25102, https://doi.org/10.1088/0022-3727/41/2/025102.
[112] M. Notomi, T. Tanabe, A. Shinya, E. Kuramochi, H. Taniyama, S. Mitsugi, M. Morita, Nonlinear and adiabatic control of highQ photonic crystal nanocavities, Opt.Express 15 (2007) 17458–17481, https://doi.org/10.1364/OE.15.017458.
[113] Y. Zhang, Y. Zhang, B. Li, Optical switches and logic gates based on self-collimated beams in two-dimensional photonic crystals, Optic Express 15 (2007) 9287, https://doi.org/10.1364/OE.15.009287.
[114] K.-Y. Lee, J.-M. Lin, Y.-C. Yang, Y.-B. Yang, J.-S. Wu, Y.-J. Lin, W.-Y. Lee, The designs of XOR logic gates based on photonic crystals, Proc. SPIE 7135 (8) (2008), https://doi.org/10.1117/12.803465, 71353Y–71353Y.
[115] H. Sharifi, S.M. Hamidi, K. Navi, A new design procedure for all-optical photonic crystal logic gates and functions based on threshold logic, Optic Commun. 370 (2016) 231–238, https://doi.org/10.1016/j.optcom.2016.03.020.
[116] S. Gholamnejad, M. Zavvari, Design and analysis of all-optical 4–2 binary encoder based on photonic crystal, Opt. Quant. Electron. (2017), https://doi.org/10.1007/s11082-017-1144-y.
[117] B. Tang, H. Dong, L. Sun, W. Zheng, Q. Wang, F. Sun, X. Jiang, A. Pan, L. Zhang, Single-mode lasers based on cesium lead halide perovskite submicron spheres, ACS Nano 11 (2017) 10681, https://doi.org/10.1021/acsnano.7b04496.
[118] R. Fenollosa, F. Meseguer, M. Tymczenko, Silicon colloids: from microcavities to photonic sponges, Adv. Mater. 20 (2008) 95–98, https://doi.org/10.1002/adma.200701589.
[119] S. Yang, Y. Wang, H. Sun, Advances and prospects for whispering gallery mode microcavities, Opt. Mater. 3 (2015) 1136–1162, https://doi.org/10.1002/adom.201500232.
[120] J.B. Chou, et al., Enabling ideal selective solar absorption with 2D metallic dielectric photonic crystals, Adv. Mater. 26 (47) (2014) 8041–8045, https://doi.org/10.1117/1.1483879.
[121] Cunlong Li, Zhigang Zang, Weiwei Chen, Zhiping Hu, Xiaosheng Tang, Wei Hu, Kuan Sun, Xianming Liu, Weimin Chen, Highly pure green light emission of perovskite CsPbBr3 quantum dots and their application for green light-emitting diodes, Optic Express 24 (2016) 15071–15078, https://doi.org/10.1364/OE.24.015071.
[122] YueLi Wang, XiaomingZhao, XinXiao, LianZeng, HaiboSun, Handong, Nonlinear Absorption and Low-Threshold Multiphoton Pumped Stimulated Emission from All-Inorganic Perovskite Nanocrystal, 2016, https://doi.org/10.1021/acs.nanolett.5b04110.
[123] W. Chen, S. Bhaumik, S. Veldhuis, et al., Giant five-photon absorption from multidimensional core-shell halide perovskite colloidal nanocrystals, Nat. Commun. 8 (2017) 15198, https://doi.org/10.1038/ncomms15198.